ROYAL SOCIETY
OF CHEMISTRY

PAPER

Check for updates

Effect of NaOH-treated sawdust incorporated in geopolymer matrix on compressive strength and adsorption property†

Gaëlle Ngnie,[a] Rock Ambela Atangana,[b] Grace Ingrid Tomou-Mbahim,[b]
Lionel Magellan Sambang,[b] Gustave Kenne Dedzo, (iD) *[b]
Hervé Kouamo Tchakoute,*[b] Claus Henning Rüscher[c] and Emmanuel Ngameni[b]

Sawdust is a multifunctional renewable biomaterial that can be incorporated into several materials to improve their properties. In the present work, the effect of sawdust incorporation in a geopolymer matrix on the compressive strength and porosity of the synthesized composite was investigated. A prior chemical treatment of sawdust with sodium hydroxide was performed to improve its compatibility with the geopolymer matrix obtained from reaction between metakaolin and sodium waterglass. Characterizations revealed an effective geopolymerization regardless the amount of sawdust added (from 0% to 10%). Compared to untreated sawdust which causes a decrease of the compressive strength, an increase of the compressive strength of the geopolymer was observed in the presence of the treated lignocellulosic material (63.04 MPa at 0% to a maximum of 75.22 MPa at 2%) followed by a decrease for higher sawdust percentage (48.48 MPa at 10%). This result confirmed the beneficial effect of the alkaline treatment of sawdust. Methylene blue (MB) was used as model cation in order to evaluate geopolymer composite porosity for cationic pollutants adsorption. Adsorption rate was found to increase with sawdust percentage in the composite, highlighting the positive effect of sawdust particles in pollutant diffusion within the network of composite materials. The diffusion coefficients increased with the percentage of sawdust in the composite materials. Preliminary work on cobalt(II) adsorption revealed good performances marked by higher and comparable adsorption capacities (in the range 0.82 to 0.90 mmol g^{-1}) regardless the amount of sawdust used in the composite.

Introduction

Geopolymer materials, especially those synthesized in alkaline medium, are increasingly considered as an interesting alternative to Portland cements, because of their low environmental footprint.[1] Regarding their structure and facile production, geopolymer materials are also increasingly used as adsorbents for the removal of pollutants in aqueous solution.[2–4] These materials are characterized by an anionic aluminosilicate backbone compensated by exchangeable cations (mainly sodium).[5] They are therefore generally used for the adsorption of cationic compounds.[4,6–8] Unfortunately,

because of their poor porosity, their use as adsorbent requests significant treatment times because of the high adsorption equilibrium times. This drawback also represents a significant limitation for application in water filtration because of fast occlusion of the membrane.[9,10] To solve this problem, it is common to use pore-forming agent (hydrogen peroxide, calcium carbonate, *etc.*) added during the synthesis of geopolymer materials in order to increase the porosity.[11–13] Unfortunately, most of these additives strongly alter the structure of resulting materials with a negative impact on mechanical properties.[14,15] The use of organic additives (such as cellulose and organic polymers) less reactive with the geopolymer materials precursors allows surface interactions without deep structural modification of the geopolymer matrix.[13,15–17] Porosity can thus be generated without significant alteration of the structure of the matrix.

Forestry industries and carpentries produce every year large amounts of sawdust generally poorly managed in African countries. This by-product of wood exploitation is indeed considered as waste in several African countries, and most often destroyed by combustion or dumped in nature.

[a] University Institute of Wood Technology of Mbalmayo, University of Yaoundé I, P. O. Box 306, Mbalmayo, Cameroon
[b] Laboratoire d'électrochimie Analytique et Génie des Matériaux, University of Yaoundé 1, P.O. Box 812, Yaoundé, Cameroun. E-mail: kennegusto@yahoo.fr
[c] Institut für Mineralogie, Leibniz Universität Hannover, Callinstrasse 3, D-30167 Hannover, Germany

† Electronic supplementary information (ESI) available: Characterization (XRD and FTIR) of precursors; optical images of composites and adsorption experiments for porosity determination. See DOI: https://doi.org/10.1039/d4lf00176a

© 2024 The Author(s). Published by the Royal Society of Chemistry

RSC Appl. Interfaces, 2024, **1**, 1241–1251 | **1241**

To overcome this environmental issue, many uses of these materials are increasingly developed in various fields (adsorption, electrochemical sensors, composite panels, energy sources and activated carbon and biochar production amongst others).[18–23] The chemical composition of this multifunctional material consisting essentially of 3 interconnected macromolecules (cellulose, hemicelluloses and lignin) allows a wide range of chemical interactions which explain these diverse applications. Recent work reveals that it is also possible to incorporate sawdust into cements and other geopolymer matrices to obtain porous and lighter materials with low thermal conductivity.[10,13,24–30] Moreover, in the specific case of geopolymer materials, the incorporation of sawdust resulted in minor modification of the mechanical resistance of the composite materials obtained. This was explained by the good dispersion of sawdust particles within the geopolymer matrix.[13] Sawdust possess many hydrogen bonds donors and acceptors functional groups (alcohol, ether, esters, phenols, *etc.*), likely to interact with the abundant oxygen atoms (hydrogen bonds acceptors) of the geopolymer matrix (Al–O–Si–O–…). According to recent works the treatment of sawdust with concentrated sodium hydroxide results in partial dissolution of lignin, followed by substantial increases of surface OH functions.[18,19] Such treatment should therefore improve the dispersion of sawdust particles within the geopolymer matrix and thus promotes favorable impact on the reinforcement of the structure of the resulting composite material while improving the diffusion of chemical species through the structure.

The dual objective of the present work is first to evaluate the role of sodium hydroxide-treated sawdust on the reinforcement of the structure of geopolymer materials. Secondly, study the impact of this additive on the porosity of the resulting composite materials for an application as an adsorbent, for cationic pollutants in aqueous media.

Practically, pristine or sodium hydroxide-treated sawdust were added at different percentages in geopolymer formulation (metakaolin and sodium waterglass). After characterization and compressive strength measurements of the composite materials, pollutants diffusion through composite materials was evaluated by adsorption of methylene blue used as a model cationic pollutant. This method consisted in exploiting the adsorption kinetics data of this cationic dye to determine the diffusion parameters (based on appropriate kinetic models) depending on the formulations considered. Methylene blue (MB) was used as the model compound because of its positive charge which ensures good adsorption by the negative geopolymer matrix. The stability in a large pH range and the easy quantification of this cationic dye were also important parameters. The study was performed on three different particle sizes (400–250 μm, 1000–400 μm and 2000–1000 μm) in order to ensure that the trends observed will remain valid regardless the particle sizes of the composite materials considered. It would thus be possible to extrapolate the results obtained to larger particles of composite materials. The most efficient materials were finally applied for cobalt ions adsorption in aqueous solution.

Materials and experimental methods

Chemicals

Sodium waterglass (molar ratio SiO_2/Na_2O of 1.6) was provided by Ingessil and cobalt nitrate hexahydrate (99%) from Aldrich. 2,2′-Bipyridine (99%), NaOH (96%) and methylene blue hydrate (MB) (≥97.0%) were purchased from Sigma-Aldrich. All other chemicals were of analytical grade.

Sawdust preparation

Sawdust was obtained from *Ayous*, a tropical soft wood. An *Ayous* sample was finely grounded and the fraction with particles diameter ranging between 100 μm and 200 μm (named S) were collected. The alkaline pre-treatment was adapted from the experimental procedure described in literature.[23] Typically, 50 g of the lignocellulosic material was dispersed in 1 L of NaOH 3 M and the mixture stirred for 18 h. The solid was recovered by filtration and thoroughly washed with deionized water until a neutral filtrate obtained. After drying in open air and then in an oven at 105 °C, the alkaline treated sawdust (TS) was stored in a sealed bag.

Metakaolin preparation

The kaolin used in this work was collected in the locality of Mayouom (West region of Cameroon) and ground for 30 min using a ball mill (MGS, Srl). The powder was sieved to obtained particles with diameter less than 125 μm. The obtained powder was calcined in an electric furnace (MGS, Srl) up to 700 °C at heating rate of 5 °C min^{-1}. An isotherm was held at 700 °C for 4 h to ensure the complete conversion of kaolin into metakaolin (named MK).

Synthesis of geopolymer composites

Geopolymer reference (named G) was prepared by mixing sodium waterglass and MK (mass ratio sodium waterglass/MK of 0.83) in a mortar for about 5 min. The homogenous paste obtained was moulded in cubic moulds (40 mm × 40 mm × 40 mm) in triplicate and cured at ambient temperature (28 °C) for 24 h. The solid samples were demoulded and sealed in a plastic bag for a 28 days curing. In the case of geopolymers–sawdust composites, a fraction of MK was replaced by S or TS to obtain mass percentages of 1, 2, 4, 7 and 10 wt%. Waterglass was added to this mixture and the geopolymers synthesised as described above. Samples obtained were named according to the type (S or TS) or the amount of the additive: G–S*x* or G–TS*x*. Where *x* (0, 1, 2, 4, 7 and 10 wt%) represents the amount of additive.

Characterization methods

The compressive strength of the geopolymer composites samples were determined according to the DIN 1164

standard on a Impact Test Equipment Limited (UK KA20 3LR), using an automatic hydraulic press with a 250 kN capacity at a constant loading rate of 0.500 MPa s^{-1}.

The XRD analyses were performed on the Bruker D8 Advance, equipped with LynXeye XE T detector detecting CuKα1,2 in Bragg–Brentano geometry with 2θ ranging from 5 to 80° (2θ). The crystalline phases were identified using X'Pert HighScore Plus software.

Fourier Transform Infrared Spectra were collected on a Bruker Vertex 80v using the KBr method. The spectra were collected on pellets prepared by mixing proper amounts of samples and KBr. The spectral resolution was set at 2 cm^{-1}.

For scanning electron microscopy (SEM) observation, the samples were first coated with gold before analysis on a Jeol XFlash 6160 Bruker Scanning Electron Microscope, operating on the secondary electron imaging (SEI) with acceleration voltage of 15.0 kV and emission current of 56.6 μA.

For optical microscope images, sawdust particles and fragments of geopolymer composites were observed using an AB instrument optical microscope equipped with a digital camera.

Points of zero charges (PZC) were determined as follow. In series of vials, 10 mL of aqueous solutions of NaNO$_3$ 0.1 M at pHs ranging between 2 and 11 were introduced. These initial pHs (pH$_i$) were controlled by adding sodium hydroxide or nitric acid aqueous solutions in vials and monitored using a pH-meter. 20 mg of treated sawdust or geopolymer materials were added in each vial, stirred for 2 h and stored at ambient. The pHs of the supernatants (pH$_f$) were recorded after two days. The PZC represents the intercept of the curve pH$_i$ − pH$_f$ = f(pH$_i$) with the abscissa.

Adsorption experiments

Methylene blue (MB) adsorption. Adsorption kinetics of methylene blue (MB) were performed in batch mode using three different particle sizes (400–250 μm, 1000–400 μm and 2000–1000 μm). Practically, 300 mg of composite material with known granulometry was dispersed in a conical flask containing 150 mL MB 5 × 10^{-5} mol L^{-1}. The suspension was stirred at constant speed of 250 rpm on an orbital shaker. At specific time intervals, approximately 1.5 mL of suspension was withdrawn with a syringe, filtered and residual MB concentration determined by UV-vis spectrophotometry at a wavelength of 664 nm. A calibration curve plotted using standard solutions of MB was used to convert absorbances into residual equivalent concentrations at specific time of the adsorption processes. Adsorption capacity at time t (Q_t (μmol g^{-1})) was determined based on MB initial concentration (C_i (μmol L^{-1})) and concentration at a given time t (C_t (μmol L^{-1})) as presented in eqn (1).

$$Q_t = \frac{(C_i - C_t)}{m} V \qquad (1)$$

where V (L) represents the volume of the solution and m (g) the adsorbent mass.

The kinetic experimental data obtained were fitted using the non-linearized forms of the pseudo-first and pseudo-second order kinetic models. The contribution of diffusion to the adsorption processes was investigated by analyzing experimental data with the external diffusion model coupled to the pore and surface mass diffusion model.

Co(II) adsorption and desorption. For cobalt adsorption, 200 mg of adsorbent was dispersed in a conical flask containing 100 mL of the metal cation 3 × 10^{-3} M and stirred on an orbital shaker at 250 rpm for 2 days. After sedimentation, the supernatant was collected and the residual amount of Co^{2+} determined using a spectrophotometer at 440 nm in presence of excess of 2,2′-bipyridine (BiPy) as complexing agent.

For desorption experiments, HCl 0.01 M, NaCl 0.01 M and BiPy (0.01 M) were used as desorption media. Typically, 25 mg of the adsorbent loaded with the metal was dispersed in 5 mL of desorption solution. The vial was sealed and stirred for 24 h at 250 rpm on an orbital shaker. The desorbed Co(II) was quantified and the desorption percentage (Des%) determined using eqn (2).

$$Des\% = \frac{C_{Des} V}{m_s \cdot Q_{Ads}} \times 100 \qquad (2)$$

where C_{Des} (μM) represents the concentration of desorbed solution, V (L) the volume of the desorption solution, m_s (g) the mass of the adsorbent loaded with cobalt and Q_{Ads} (mol L^{-1}) the amount of Co(II) loaded on the adsorbent.

Results and discussion

Characterization of geopolymer composites

X-ray patterns. The X-ray patterns of the geopolymer composites without sawdust (G) or using untreated sawdust (G–S2 and G–S10) and treated sawdust (G–TS2 and G–TS10) as an additive are displayed in Fig. 1. These patterns showed similar trends and indicated well-defined peaks of illite, quartz and anatase. In addition to these crystalline phases, the XRD patterns of all geopolymer composites depicted the broad hump ranging from 18° to 38° 2θ belonging to the formation of the binder in the structure of geopolymer composites. The X-ray pattern of metakaolin showed similar halo of diffraction between 15 and 30° 2θ (see ESI,† Fig. S1). The shift toward higher 2θ in the case of synthesized geopolymer composites was ascribed to the formation of the binder, due to the reaction between metakaolin and sodium waterglass.[31]

These results are a proof that the presence of sawdust does not significantly modify the reaction between metakaolin and sodium waterglass. Sawdust thus mainly act as a simple additive with minor contribution on the chemical processes that occurred during geopolymerization.

Infrared spectra. Fig. 2 depicts the infrared spectra of geopolymer composites without sawdust (G) or using untreated sawdust (G–S2 and G–S10) and treated sawdust (G–TS2 and G–TS10) as an additive. All the spectra show the
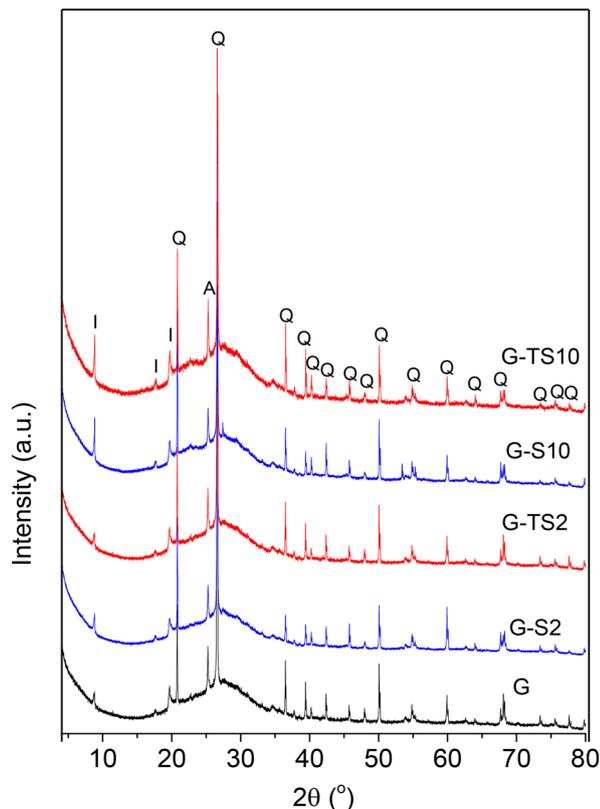
© 2024 The Author(s). Published by the Royal Society of Chemistry

RSC Appl. Interfaces, 2024, **1**, 1241–1251 | **1243**

Fig. 1 X-ray patterns of geopolymer and geopolymer–sawdust composites.

absorption bands between 439 and 450 cm^{-1}, attributed to the bending vibration modes of Si–O bonds.[32] The absorption bands located at 681–683 cm^{-1} are assigned to the bending vibration modes of Si–O of quartz.[33,34] The absorption bands located at 853–862 cm^{-1} are due to the bending vibration modes of Si–OH of silanol groups.[35] The symmetrical stretching vibration of sialate bonds (Si–O–Al) bonds appears at 715–712 cm^{-1} on the spectra of geopolymer composites.
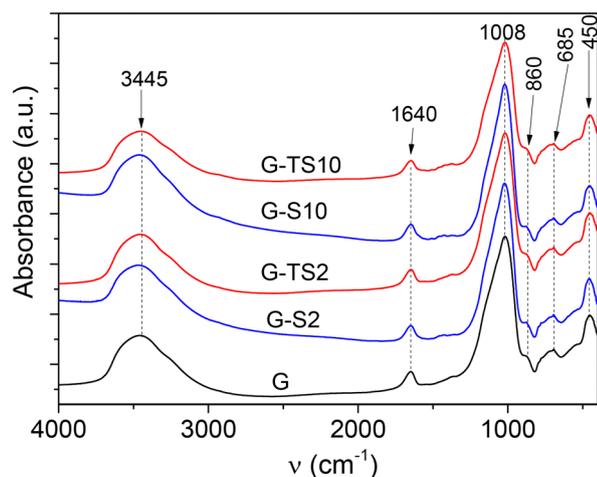

Fig. 2 FTIR spectra of geopolymer and geopolymer–sawdust composites.

The OH and H–O–H stretching and bending vibrations of hydrogen-bonded water molecules appear on the spectra of all geopolymer composites at 3435–3445 cm^{-1} and 1638–1640 cm^{-1}, respectively. The symmetric and asymmetric stretching vibration modes of Si–O–Si and Si–O–Al are observed at 1007–1008 cm^{-1} on the spectra of geopolymer composites. This band is observed at 1072 cm^{-1} on the spectrum of metakaolin (see ESI,† Fig. S2). The shift of this absorption band towards lower wavenumber on the infrared spectra of geopolymer composites was due to the dissolution of metakaolin followed by the polycondensation process. This confirmed the formation of –Si–O–Si–O–Si–O–Al– chains in the geopolymer composites.

The FTIR spectra of pristine and sodium hydroxide treated sawdust (Fig. S3†) showed the typical bands reported in literature and assigned to the presence of the main lignocellulosic material macromolecules (cellulose, hemicelluloses and lignin).[19,23] The broad band at 2891 cm^{-1} was assigned to C–H bonds of aliphatic groups, the intense band at 1027 cm^{-1} attributed to C–O bonds of alcohol groups and ether bonds.

The bands at 3340 cm^{-1} and 1648 cm^{-1} were assigned to physisorbed water molecules. These bands were not present in the spectra of composite material, certainly because of the law relative abundance of additive in the materials. Meanwhile, almost perfectly superimposed FTIR spectra of composite materials regardless the nature and the percentage of incorporated lignocellulosic material once again confirmed that the geopolymerization process was poorly affected by the presence of the organic compound.

SEM micrograph images. Fig. 3 depicts the SEM images observed at the magnification 500× and 5000× of the geopolymer and composites obtained with treated and untreated sawdust particles.

It can be observed that the geopolymer material without sawdust addition showed a coarse microstructure while the images of geopolymer composites after incorporation of 2 wt% of untreated or treated sawdust displayed a more homogeneous, compact and denser matrices. Samples containing 10 wt% of additive showed heterogeneous microstructures, certainly due to the excess of sawdust that prevents long range geopolymerization. These sawdust particles (highlighted by red rectangles in Fig. 3) appeared as thin fibers, reminiscent of vegetal cells.

Compressive strengths. The compressive strength values of the geopolymer composites using untreated and treated sawdust are presented in Fig. 4.

The compressive strengths of metakaolin-based geopolymer composites using untreated sawdust as an additive decreased when the amount of the lignocellulosic material in the formulation (from 63.04 MPa at 0% to 52.01 MPa at 7%) was increased. These results indicate the loss of this mechanical property, certainly due to the less important compressive strength of *Ayous* sawdust (36.62 MPa parallel to fibers)[36] compared to that of the geopolymer matrix. When NaOH-treated sawdust was used as an additive, the
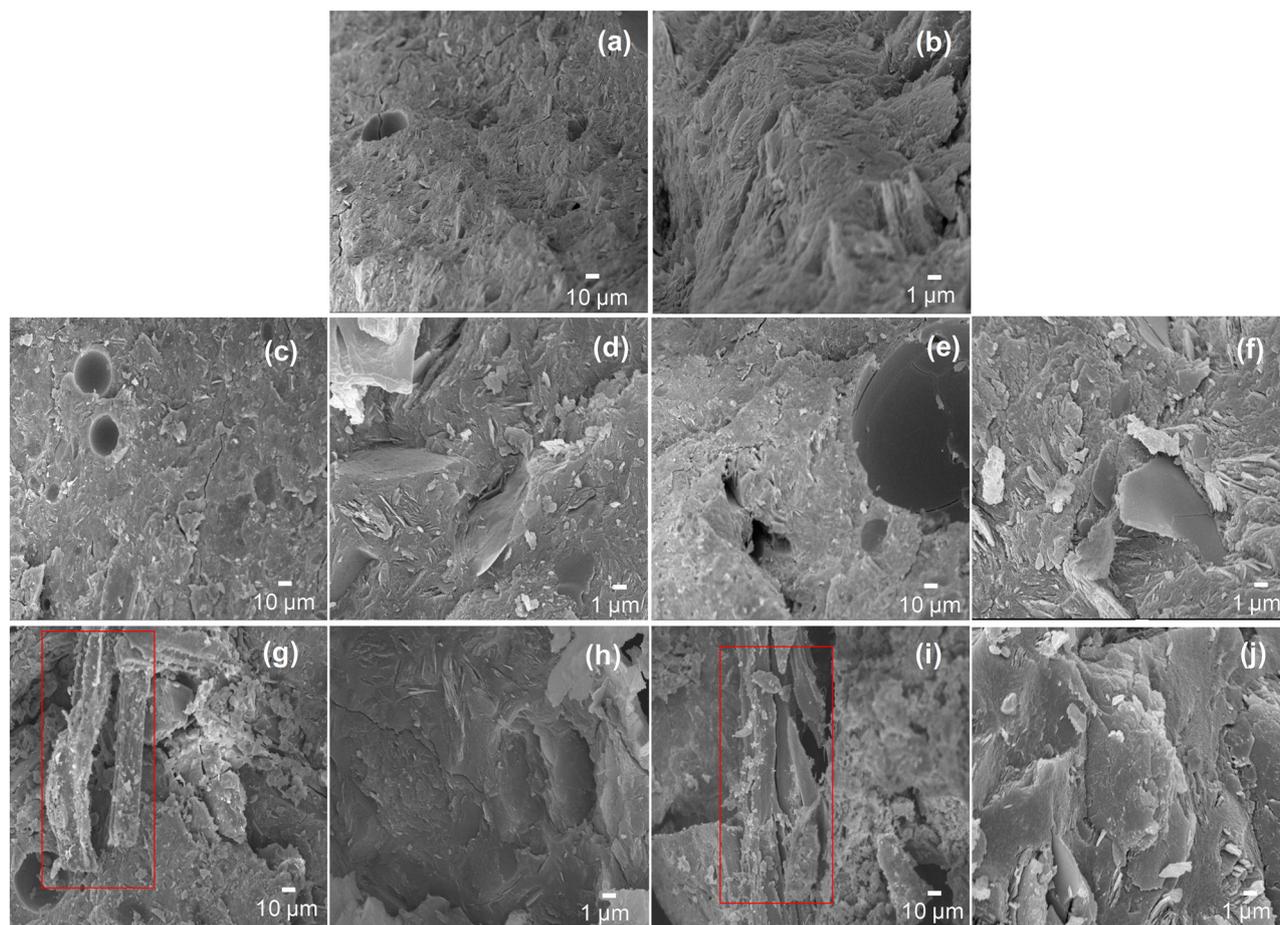
Fig. 3 SEM pictures of geopolymer and geopolymer–sawdust composites at two magnifications (×500 and ×5000). (a) and (b) G, (c) and (d) G–TS2, (e) and (f) G–S2, (g) and (h) G–TS10 and (i) and (j) G–S10.

compressive strength first increased with the amount of filler (from 63.04 MPa at 0% to 75.22 MPa at 2%). This was followed by the lowering of the compressive strength (48.48 MPa) at 10%. The increase of compressive strength could be due to the strong interaction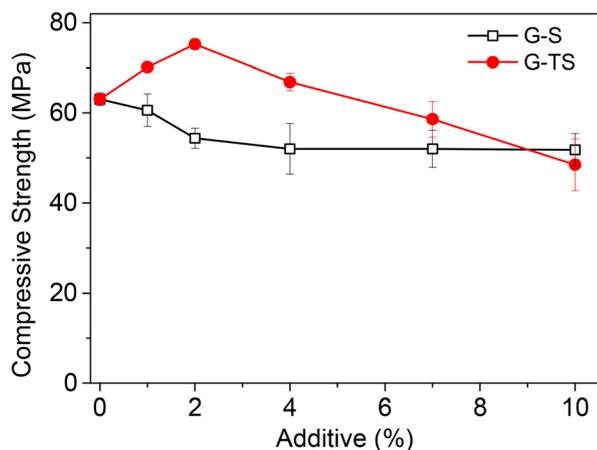s between sawdust particles and the geopolymer matrix. These interactions could be of hydrogen bonding type between the hydroxyl functionalities of sawdust particles (hydrogen-bonds donor and acceptors) and the oxygen atoms (hydrogen bonds acceptors) of the –Si–O–Si–O–Si–O–Al– chains.

Compared to untreated sawdust particles, the NaOH treatment resulted in an increase of the surface OH groups, due to partial delignification of the lignocellulosic material. These interactions favoured the homogenous distribution of sawdust particles in the matrix and then promote the increase of the compressive strength. The optical microscope images of the composite materials presented in Fig. S4† confirmed the good dispersion of sawdust particles in the geopolymer matrix. Despite these favourable interactions, a significant amount of sawdust in the composite resulted in a decrease of the compressive strength probably because of the poor long-range polymerization observed.

The compressive strengths obtained in this work were compared with those of some geopolymer–biomass composites found in the literature (Table 1).

These composites generally present lower compressive strength values compared to those recorded in this work.

Fig. 4 Compressive strength values of geopolymer and geopolymer–sawdust composites.

© 2024 The Author(s). Published by the Royal Society of Chemistry

RSC Appl. Interfaces, 2024, **1**, 1241–1251 | **1245**

Table 1 Compressive strength of some geopolymer–biomass composites found in the literature

Biomass	Biomass (%)	Compressive strength (MPa)	Ref.
Spirulina platensis	3	14.7	37
Tetraselmis suecica	1	16.1	37
Cork waste	20	15.84	38
Abaca fiber	1	25.9	39
Cellulose	5	36.22	40
Sawdust	20	65	16
Sawdust	20	16.04	27
Sawdust	1	60.59	This work
NaOH treated sawdust	2	75.22	This work

This could be due not only to the alkaline treatment, but also to the small size of the sawdust particles used as additive.

Effect of the amount of sawdust on methylene blue diffusion through composites

Only the composites obtained with NaOH-treated sawdust was used in this section, due to the excellent mechanical properties displayed.

General trends of kinetic curves. MB adsorption kinetics curves on different composite materials with particle sizes 400–250 μm, 1000–400 μm and 2000–1000 μm are plotted in Fig. 5. Regardless the particle size considered and composite material composition, the curves were characterized by a fast increase of the adsorption capacity at the beginning of the processes. This was followed by a gradual decrease of the adsorption rate till the formation of a plateau. The fast increase of the adsorption capacity was due to the good availability of surface adsorption sites.
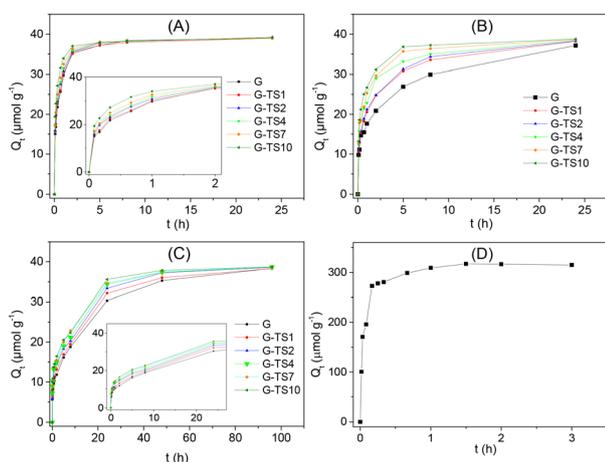

Fig. 5 Methylene blue adsorption kinetics curves on different composite materials with particle sizes (A) 400–250 μm, (B) 1000–400 μm and (C) 2000–1000 μm. Experimental conditions: methylene blue 200 μmol L^{-1}, composite material 2 g L^{-1} and stirring at ambient temperature (25 °C) at 250 rpm. Curve (D) was recorded at identical experimental conditions with only sawdust 0.2 g L^{-1} as adsorbent. Insets of (A) and (C), kinetic curves during the first stages of adsorption.

The decrease of the adsorption rate was assigned to the implication of the less available inner adsorption sites. The formation of the plateau indicates the achievement of the equilibrium marked by the saturation of the entire adsorption sites. The shape of these different domains depends both on the sawdust amounts in the composite materials and on the particle size. Thus, regarding the amount of sawdust in the composite, adsorption on the pure geopolymer was the slowest process. The presence of increasing amounts of sawdust facilitates the adsorption process, marked by a faster formation of the plateau. The presence of sawdust therefore seems to accelerate the adsorption process. The increase of particles size resulted in the increase of the time required to reach equilibrium. In the case of G, 10 h, 24 h and 92 h were necessary to reach equilibrium for particles sizes 400–250 μm, 1000–400 μm and 2000–1000 μm respectively.

The kinetic curve obtained using only sawdust (0.2 g L^{-1}) equivalent to that present in G–TS10 is presented in Fig. 5(D). This curve showed a fast adsorption process (equilibrium reached after only 1 hour) and maximum adsorption capacity at least 9 times greater than that obtained with composite materials. The difference observed compared to composite materials was explained by the higher performance of sawdust compared to geopolymer, for the adsorption of this dye.

For efficient analysis of the experimental data, classical kinetic models (pseudo-first and pseudo-second order kinetic models) and those allowing the interpretation of the diffusion processes (surface diffusion and surface and internal diffusion models) were applied.

Classical adsorption kinetic models. Pseudo-first and pseudo-second order kinetic models (eqn (3) and (4) respectively), widely used for the analysis of adsorption processes, were applied for experimental data fitting.[41–43]

$$Q_t = Q_e\left(1 - e^{-k_1 t}\right) \tag{3}$$

$$Q_t = \frac{k_2 Q_e^2 t}{1 + k_2 Q_e t} \tag{4}$$

where Q_t (μmol g^{-1}), is the adsorption capacity of MB at time t (h), Q_e (μmol g^{-1}), adsorption capacity of MB at the equilibrium, k_1 (h^{-1}) the pseudo-first order rate constant and k_2 (g μmol^{-1} h^{-1}) the pseudo-second order rate constant.

The non-linear fitting obtained from the experimental data recorded on different composites of different particles size, are presented as ESI† (Fig. S5). The constants extracted from these curves were summarized in Table S1.† The pseudo-second-order model was found more suitable for data analysis (R^2 in the range 0.84 to 0.99) compared to the pseudo-first order model (R^2 in the range 0.77 to 0.87). Initial adsorption rates (h determined from eqn (5)) obtained from this model was compared to evaluate the impact of the particles size and the percentage of sawdust within the composite material on the adsorption process.

1246 | *RSC Appl. Interfaces*, 2024, **1**, 1241–1251

© 2024 The Author(s). Published by the Royal Society of Chemistry

$$h = K_2 q_e{}^2 \qquad (5)$$

The variation of the initial adsorption rate as a function of particles size and the amount of sawdust in the composites are presented in Fig. 6.

The initial adsorption rates decreased when particles size was increased. This trend was due to the poor availability of adsorption sites when the particle sizes of adsorbents increase. The adsorption sites close to the surface of the particles were easily accessible because of the fast diffusion of the adsorbate. This phenomenon was confirmed by the important equilibrium time recorded for the larger particles (Fig. 5). Furthermore, the initial adsorption rates increased with the amount of sawdust in the composites. The presence of sawdust improved the accessibility of adsorption sites to MB. This result can be rationalized by considering the greater porosity of sawdust compared to geopolymer that facilitates the diffusion of the adsorbate within the composite materials. The high value of the initial adsorption rate recorded on sawdust (8789 $\mu mol\ g^{-1}\ h^{-1}$) at least 25 times greater than those obtained on composite materials confirmed this hypothesis.

Considering the importance of the adsorbate diffusion process towards variable particles size and different composite materials formulations, the experimental kinetic data were analyzed using kinetic models essentially based on diffusion.

Kinetic models for diffusion studies. The contribution of surface and internal diffusion during MB adsorption of on composites materials were determined using external surface diffusion kinetic model (eqn (6) and (7)) and surface and internal diffusion model (eqn (8)).[44]

$$\ln \frac{C_t}{C_i} = -k_f \frac{S}{V} t \qquad (6)$$
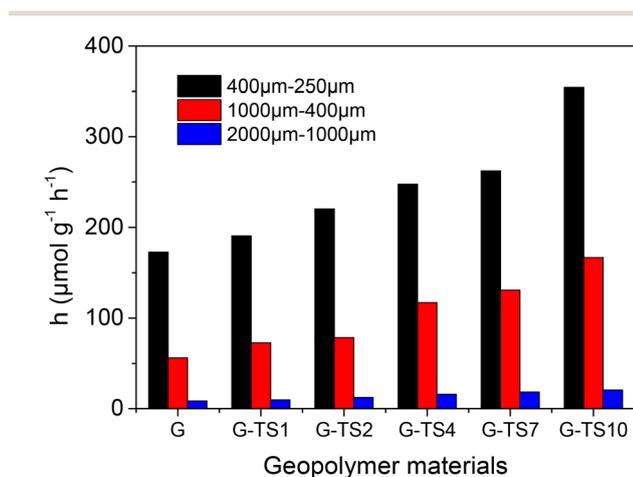
$$\frac{S}{V} = \frac{3m}{\rho d} \qquad (7)$$

$$-\log\left(1 - \left(\frac{q_t}{q_e}\right)^2\right) = \left(\frac{4\pi^2 D}{2.3 d^2}\right) t \qquad (8)$$

where S (cm^2) represents the total interfacial surface of the particles, V (cm^3) the total volume of the solution, m ($g\ cm^{-3}$) the adsorbent concentration, d (cm) the mean diameter of adsorbent particles and ρ ($g\ cm^{-3}$) the apparent density of the material considered.

The plots obtained by applying linear transformations of these models on experimental data are presented as ESI† (Fig. S6). The constants obtained from these curves were summarized in Table S2.†

To facilitate the analysis of the results obtained, the values of the surface diffusion equilibrium constants and the diffusion coefficients were plotted in Fig. 7 as a function of particles size and the amount of sawdust in the composite materials. The surface mass transfer does not seem to be strongly affected by the presence of sawdust in the geopolymer or by the particle size of the composites. Regardless the particles size, minor variations were observed
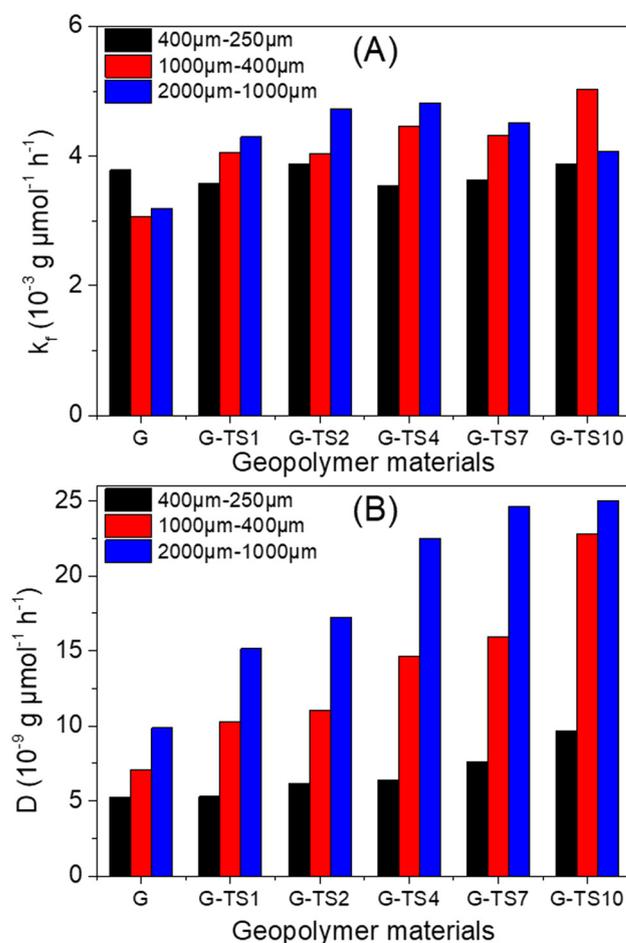

Fig. 7 Variations of (A) surface diffusion equilibrium constants and (B) diffusion coefficients as function of particles size and the amount of sawdust in the composite materials.

Fig. 6 Variation of initial adsorption rate as a function of particles size and the amount of sawdust in the composites.

(k_f values were in the range 3.55×10^{-3} cm s^{-1} and 4.82×10^{-3} cm s^{-1}). This could be explained by the fact that k_f is determined from experimental data obtained during surface adsorption of MB.

In the present case, small amounts of an additive should have almost no effect on the adsorption at surface sites. Therefore, only the geopolymer matrix was expected to dominate the surface mass transfer. This hypothesis was confirmed when considering the k_f value of *Ayous* sawdust alone (17.64×10^{-3} cm s^{-1}), at least 3 times higher than that of composite materials.

Regarding the values of diffusion coefficient (D), there was a strong increase when considering both the particles size and the amount of sawdust in the composites. The presence of sawdust therefore promotes the diffusion of the adsorbate within the materials. Since the lignocellulosic material was less compact than the geopolymer phase, its particles dispersed within the materials facilitate MB diffusion within the materials. This diffusion was also improved by the good distribution of the sawdust particles within the geopolymers (even GP-S10 showed no sawdust particles agglomeration) as showed by optical microscope images (Fig. S4†).

The increase of the value of D with the particles size was due to the greater contribution of internal diffusion when the particle size increases. Indeed, D is the sum of the contributions of the surface and internal diffusions.

B_N (Biot number) values (eqn (9)) were determined from k_f and D values (Table S2†) to identify the type of diffusion that controls the adsorption process.

$$B_N = k_f \frac{d}{D} \tag{9}$$

These values were above 100, indicating that compared to the external surface diffusion, it is internal diffusion that controls MB adsorption.[18]

Application for cobalt(II) removal

The management of water pollution by heavy metals represents an actual environmental concern. Cobalt holds an important place among this class of contaminants regarding its implication in several technological and industrial fields such as electronics, batteries, production of specialized alloys, pigments synthesis amongst other.[45–47] Cobalt mining, metal production followed by these diverse applications naturally results in environmental pollution. The development of effective depollution processes thus represents a major challenge.[48–51] The ability of the composite materials synthesized in this work to adsorb cations has been exploited for the adsorption of Co(II) ions in aqueous solution.

The variation of Co(II) adsorption capacity as a function of adsorbent type (treated sawdust, geopolymer or geopolymer composites) is depicted in Fig. 8(A). Only the geopolymer composites with particle size 400–250 μm were used for these experiments. Minor variations were observed on the
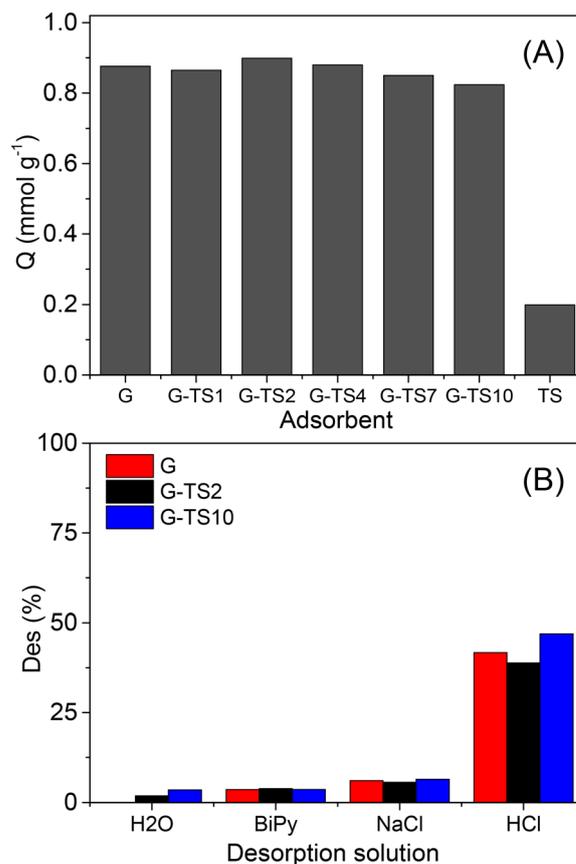

Fig. 8 (A) Variation of Co(II) adsorption capacity of treated sawdust (TS), geopolymer and geopolymer–sawdust (treated and untreated) composites with particle sizes 400–250 μm. Experimental conditions: 0.2 g of adsorbent in 100 mL of Co(II) 3 mM, stirred for two days at 250 rpm. (B) Co(II) desorption percentages as a function of desorption solution. Experimental conditions: 2.5 mg of loaded adsorbent in 5 mL of desorbing solution, stirred at 250 rpm for 1 day.

performances of composite materials as the adsorption capacities values were ranging between 0.82 mmol g^{-1} (for G–TS10) to 0.90 mmol g^{-1} (for G-TS2). These performances even not fully optimized were relatively highest compared to low-

Table 2 Comparison of the performances of some adsorbent for cobalt(II) adsorption

Adsorbent	Q (mg g^{-1})	Ref.
γ-Alumina	75.78	49
Multi-walled carbon nanotubes	78.94	49
Modified polymeric adsorbents	61.34	52
Pre-treated 2-*Hypnea valentiae* algae	16.66	53
Montmorillonite	6.92	54
Aminated graphene oxide	116.35	55
Mesoporous silica composite	185.23	56
Raw shrimp shells	7.692	57
NaOH activated slag based geopolymer	91.21	58
KOH activated slag based geopolymer	192.31	58
Pyrophyllite based geopolymer	7.18	59
Metakaolin based geopolymer	69.23	60
Sawdust	11.74	This work
Sawdust–geopolymer composite	48.51–51.84	This work

1248 | *RSC Appl. Interfaces*, 2024, **1**, 1241–1251

© 2024 The Author(s). Published by the Royal Society of Chemistry

cost adsorbent presented in the literature. Meanwhile adsorbent based on slag geopolymer or modified graphene, showed comparable or higher adsorption capacities (see Table 2).

Surprisingly, the adsorption capacity reported in the case of treated sawdust (0.20 mmol g^{-1}) was at least 4 times less important. These results showed poor correlation with MB adsorption data, where the opposite trend was observed, marked by the highest performance with TS. This indicates that the adsorption of the two cationic compounds on geopolymer and geopolymer-composite materials occurs through different mechanisms. Thus, the ion exchange between the exchangeable cations of the geopolymer and the Co(II) in solution could not solely explain the high performance obtained. It is well-known that geopolymers synthesized with alkaline activators are generally basic. This property was confirmed in the present work by experimental values of points of zero charge (PZC) ranging between 9.67 (for G) and 10.29 (for G–TS10) (see ESI,† Fig. S7), confirming the presence of basic surface groups. During adsorption, these basic groups certainly favored the microprecipitation of Co(II) as hydroxides (Co(OH)$_2$) (with solubility constant (K_s) of 13×10^{-15}) inside the pores of the geopolymers, and thus explained the significant adsorption capacities obtained. Similar mechanism during heavy metals removal by adsorption was reported in the literature.[61,62] TS on the other hand showed the lowest PZC (7.62) that could not allow Co(II) surface precipitation.

The desorption of adsorbed Co(II) was performed in order to evaluate the potential reuse of the adsorbents. 0.01 M aqueous solutions of HCl, NaCl and BiPy were used as desorption media. For comparison purposes, deionized water was also used as desorption medium. The results obtained are presented in Fig. 8(B). Deionized water, NaCl and BiPy solutions showed minor Co(II) desorption as indicated by the values of desorption percentages, lower than 6.5%. These results indicate the strong adsorption of Co(II) on geopolymer materials. Moreover, the poor performance of NaCl solution confirmed that Co(II) adsorption onto geopolymer was not a simple cation exchange process. The use of HCl solution, on the other hand afforded higher desorption percentages (around 40%). This result can be explained by the solubilization of the cobalt hydroxide present at the surface of the geopolymer materials, by the acidic solution. This result therefore confirmed the adsorption of Co(II) on geopolymer materials as hydroxides. However, the desorption percentages recorded remained low to justify the reuse of adsorbents. The use of a more concentrated acid solution could be required, but would result in the degradation of the geopolymer materials.

Conclusion

The dual objective of the present work was to evaluate the effect of sodium hydroxide-treated sawdust on the reinforcement of the structure of a geopolymer material (obtained from reaction between metakaolin and sodium waterglass) and to study the contribution of this natural and renewable additive on the porosity of the resulting composite materials Series of geopolymer materials containing varying amounts of sawdust were first successfully synthesized as indicated by the good dispersion of sawdust particles and the formation of sialate and siloxo bonds. An improvement of the compressive strength was observed for small amounts of pretreated sawdust (maximum value obtained at 2%) added in the formulations. Methylene blue adsorption was used efficiently to evaluate the impact of sawdust on the diffusion of cationic compounds within the geopolymer structure. The presence of treated-sawdust increases the porosity of the geopolymer as indicated by the increase of MB adsorption rate and diffusion coefficients. A preliminary work on Co(II) ions adsorption revealed good performances marked by higher and comparable adsorption capacities regardless the amount of sawdust used in the composite. The present work therefore demonstrates that sawdust can be effectively used as reinforcing material to improve not only the compressive strength but also to enhance and control the porosity of geopolymers for applications in adsorption. In the future, it would be interesting to study the effects of pretreated sawdust on other essential mechanical properties of geopolymers as well as adsorption of other heavy metals. Interestingly, the difficult desorption of the adsorbed Co(II) ions suggests a potential use for the sequestration (immobilization) of radioactive waste and other harmful metal cations.

Data availability

The data supporting this article have been included as part of the ESI.†

Conflicts of interest

There are no conflicts to declare.

Acknowledgements

Notes and references

1 M. F. Noor-ul-Amin, K. Muhammad and S. Gul, *J. Cleaner Prod.*, 2016, **129**, 491–495.

2 L. Li, S. Wang and Z. Zhu, *J. Colloid Interface Sci.*, 2006, **300**, 52–59.

3 İ. Kara, D. Yilmazer and S. T. Akar, *Appl. Clay Sci.*, 2017, **139**, 54–63.

4 K. Liang, X. Q. Wang, C. L. Chow and D. Lau, *J. Environ. Manage.*, 2022, **322**, 116066.

5 J. L. Provis and J. S. J. Van Deventer, *Geopolymers: structures, processing, properties and industrial applications*, Woodhead, Oxford, 2009.

© 2024 The Author(s). Published by the Royal Society of Chemistry

RSC Appl. Interfaces, 2024, **1**, 1241–1251 | **1249**

6 T. Cheng, M. Lee, M. Ko, T. Ueng and S. Yang, *Appl. Clay Sci.*, 2012, **56**, 90–96.

7 F. J. López, S. Sugita and T. Kobayashi, *Chem. Lett.*, 2013, **43**, 128–130.

8 F. J. López, S. Sugita, M. Tagaya and T. Kobayashi, *J. Mater. Sci. Chem. Eng.*, 2014, **02**, 07.

9 A. Naveed, S. F. Noor-ul-Amin, M. Khraisheh, M. Al Bakrid and S. Gul, *Desalin. Water Treat.*, 2019, **161**, 126–131.

10 M. Youmoue, R. T. T. Fongang, A. Gharzouni, R. C. Kaze, E. Kamseu, V. M. Sglavo, I. K. Tonle, B. Nait-Ali and S. Rossignol, *SN Appl. Sci.*, 2020, **2**, 642.

11 X. Zang, C. Bai, Y. Qiao, X. Wang, D. Jia, H. Li and P. Colombo, *Composites, Part A*, 2021, **150**, 106629.

12 B. Panda, S. C. Paul, L. J. Hui, Y. W. D. Tay and M. J. Tan, *J. Cleaner Prod.*, 2017, **167**, 281–288.

13 L. Yan, B. Kasal and L. Huang, *Composites, Part B*, 2016, **92**, 94–132.

14 H. R. Rasouli, F. Golestani-Fard, A. R. Mirhabibi, G. M. Nasab, K. J. D. MacKenzie and M. H. Shahraki, *Ceram. Int.*, 2015, **41**, 7872–7880.

15 M. C. Acar, A. I. Celik, R. Kayabası, A. Sener, N. Özdöner and Y. O. Özkılıc, *J. Mater. Res. Technol.*, 2023, **24**, 81–89.

16 P. Duan, C. Yan, W. Zhou and W. Luo, *Constr. Build. Mater.*, 2016, **111**, 600–610.

17 N. Ranjbar and M. Zhang, *Cem. Concr. Compos.*, 2020, **107**, 103498.

18 C. P. Nanseu-Njiki, G. K. Dedzo and E. Ngameni, *J. Hazard. Mater.*, 2010, **179**, 63–71.

19 G. K. Dedzo, C. P. Nanseu-Njiki and E. Ngameni, *Talanta*, 2012, **99**, 478–486.

20 C. B. Njine-Bememba, G. K. Dedzo, C. P. Nanseu-Njiki and E. Ngameni, *Holzforschung*, 2015, **69**, 347–356.

21 B. N. Ngana, G. K. Dedzo, C. P. Nanseu-Njiki and E. Ngameni, *Electroanalysis*, 2019, **31**, 383–389.

22 B. N. Ngana, P. M. T. Seumo, L. M. Sambang, G. K. Dedzo, C. P. Nanseu-Njiki and E. Ngameni, *J. Environ. Chem. Eng.*, 2021, **9**, 104984.

23 L. M. Sambang, G. K. Dedzo, S. Rigolet and E. Ngameni, *Sustainable Chem. Pharm.*, 2023, **33**, 101068.

24 E. P. Aigbomian and M. Fan, *Constr. Build. Mater.*, 2013, **40**, 361–366.

25 D. Dai and M. Fan, *Ind. Crops Prod.*, 2015, **74**, 417–424.

26 V. Corinaldesi, A. Mazzoli and R. Siddique, *Constr. Build. Mater.*, 2016, **123**, 281–289.

27 D. C. Pereira, G. Amaral-Labat and G. F. B. S. Lenze, *Ceramica*, 2019, **65**, 104–109.

28 H. Ye, B. Asante, G. Schmidt, A. Krause, Y. Zhang and Z. Yu, *J. Cleaner Prod.*, 2023, **420**, 138381.

29 A. Sales, F. R. Souza, W. N. Santos, A. M. Zimer and F. C. R. Almeida, *Constr. Build. Mater.*, 2010, **24**, 2446–2453.

30 A. Sales, F. R. Souza and F. C. R. Almeida, *Constr. Build. Mater.*, 2011, **25**, 2793–2798.

31 S. Jurado-Contreras, E. Bonet-Martínez, P. J. Sánchez-Soto, O. Gencel and D. Eliche-Quesada, *Arch. Civ. Mech. Eng.*, 2022, **22**, 121.

32 A. Tironi, M. A. Trezza, A. N. Scian and E. F. Irassar, *Constr. Build. Mater.*, 2012, **28**, 276–281.

33 H. K. Tchakouté, C. H. Rüscher, J. N. Y. Djobo, B. B. D. Kenne and D. Njopwouo, *Appl. Clay Sci.*, 2015, **107**, 188–194.

34 A. K. Kronenberg, H. F. B. Hasnan, C. W. Holyoke III, R. D. Law, Z. Liu and J. B. Thomas, *Solid Earth*, 2017, **8**, 1025–1045.

35 Z. Ghasemi and H. Younesi, *Waste Biomass Valoriz.*, 2012, **3**, 61–74.

36 E. Gennari, R. Picchio, D. Tocci and A. L. Monaco, *Environ. Sci. Proc.*, 2021, **3**, 27.

37 E. Agnoli, R. Ciapponi, M. Levi and S. Turri, *Materials*, 2019, **12**, 1004.

38 A. Sudagar, S. Andrejkovičová, C. Patinha, A. Velosa, A. McAdam, E. F. da Silva and F. Rocha, *Appl. Clay Sci.*, 2018, **152**, 196–210.

39 R. A. J. Malenab, J. P. S. Ngo and M. A. B. Promentilla, *Materials*, 2017, **10**, 579.

40 H. Ye, Y. Zhang, Z. Yu and J. Mu, *Constr. Build. Mater.*, 2018, **173**, 10–16.

41 Y. S. Ho and G. Mckay, *Resour., Conserv. Recycl.*, 1999, **25**, 171–193.

42 Y. Liu and Y. J. Liu, *Sep. Purif. Technol.*, 2008, **61**, 229–242.

43 Q. Li, L. Chai, Z. Yang and Q. Wang, *Appl. Surf. Sci.*, 2009, **255**, 4298–4303.

44 N. Dizge, C. Aydiner, E. Demirbas, M. Kobya and S. Kara, *J. Hazard. Mater.*, 2008, **150**, 737.

45 J. Edel, G. Pozzi, E. Sabbioni, R. Pietra and S. Devos, *Sci. Total Environ.*, 1994, **150**, 233–244.

46 D. Barałkiewicz and J. Siepak, *Pol. J. Environ. Stud.*, 1999, **8**, 201–208.

47 B. L. Finley, A. D. Monnot, S. H. Gaffney and D. J. Paustenbach, *J. Toxicol. Environ. Health*, 2012, **15**, 493–523.

48 T. Dewangan, A. Tiwari and A. Bajpai, *J. Dispersion Sci. Technol.*, 2009, **30**, 56–60.

49 M. H. Dehghani, K. Yetilmezsoy, M. Salari, Z. Heidarinejad, M. Yousefi and M. Sillanpää, *J. Mol. Liq.*, 2020, **299**, 112154.

50 P. Yang, J. Wang, S. Wang, C. Yang, P. Zhao, B. Huang, Q. Wang and H. Wang, *ACS Omega*, 2022, **7**, 37452–37464.

51 A. Irshad, M. Atif, A. Ghani, B. Ali, S. A. Ahmad and M. Alex, *Sci. Rep.*, 2023, **13**, 7356.

52 F. Maleki, M. Gholami, R. Torkaman, M. Torab-Mostaedi and M. Asadollahzadeh, *Environ. Technol. Innovation*, 2021, **24**, 102054.

53 L. Vafajoo, R. Cheraghi, R. Dabbagh and G. Mckay, *Chem. Eng. J.*, 2018, **331**, 39–47.

54 W. Hu, S. Lu, W. Song, T. Chen, T. Hayat, N. S. Alsaedi, C. Chen and H. Liu, *Appl. Clay Sci.*, 2018, **157**, 121–129.

55 F. Fang, L. Kong, J. Huang, S. Wu, K. Zhang, X. Wang, B. Sun, Z. Jin, J. Wang, X. Huang and J. Liu, *J. Hazard. Mater.*, 2014, **270**, 1–10.

56 R. Awual, M. Hasan, A. Islam, A. M. Asiri and M. M. Rahman, *J. Mol. Liq.*, 2020, **298**, 112035.

57 G. Gök, H. Kocyigit, O. Gök and H. Celebi, *Chem. Eng. Res. Des.*, 2022, **186**, 229–240.

58 Q. Su, L. Deng, Q. Ye, Y. He and X. Cui, *ACS Omega*, 2020, **5**, 23898–23908.

59 L. Panda, S. S. Rath, D. S. Rao, B. B. Nayak, B. Das and P. K. Misra, *J. Mol. Liq.*, 2018, **263**, 428–441.

60 I. Kara, D. Tunc, F. Sayin and S. T. Akar, *Appl. Clay Sci.*, 2018, **161**, 184–193.

61 N. A. A. Qasem, R. H. Mohammed and D. U. Lawal, *npj Clean Water*, 2021, **4**, 36.

62 P. Arokiasamy, M. M. A. B. Abdullah, S. Z. A. Rahim, M. Sadique, L. Y. Ming, M. A. A. M. Salleh, M. R. R. M. A. Zainol and C. M. R. Ghazali, *J. Mater. Res. Technol.*, 2023, **22**, 126–156.

© 2024 The Author(s). Published by the Royal Society of Chemistry

RSC Appl. Interfaces, 2024, **1**, 1241–1251 | **1251**